Physicochem. Probl. Miner. Process., 62(7), 2026, 237557

http://www.journalssystem.com/ppmp

Physicochemical Problems of Mineral Processing

ISSN 1643-1049

Short-range acid–base (hydration) forces as a dominant control on albite/orthoclase flotation selectivity: a colloidal-probe AFM and extended-DLVO study

Muhammed Fatih Can [1], Cengiz Karagüzel [2]

[1] Department of Mining Engineering, Faculty of Engineering, Afyon Kocatepe University, Afyonkarahisar, Türkiye

[2] Department of Mining Engineering, Faculty of Engineering, Kütahya Dumlupınar University, Kütahya, Türkiye

Corresponding author: cengiz.karaguzel@dpu.edu.tr (C. Karagüzel)

Abstract: Selective flotation of albite from potassium feldspar (microcline/orthoclase) with cationic collectors is controlled by monovalent salt, yet the surface forces responsible have been inferred from electrokinetic and thermodynamic data rather than measured directly. Here we probe these interactions by colloidal-probe atomic force microscopy (AFM), interpreted through classical and extended DLVO theory. Force curves between a silica microsphere and polished albite and orthoclase surfaces were acquired versus NaCl and at the separation condition. Constant-potential DLVO fits returned Debye lengths of the expected order, and effective potentials reproducing the electrokinetic ordering (albite more negative than orthoclase) and, at high ionic strength, resolving a mineral-distinguishing difference absent from the zeta potentials. Surface free-energy components from thin-layer wicking resolved the forces into Lifshitz–van der Waals, double-layer, and Lewis acid–base contributions. Added electrolyte shortened the force range through double-layer compression, while a non-DLVO short-range repulsion re-emerged at high ionic strength. At the separation condition, albite showed a stronger short-range repulsion than orthoclase; a rigorous van Oss decomposition attributes this to a repulsive acid–base (hydration-type) force more than twice as strong on albite, mirroring selectivity, whereas a simplified rule returns an attractive term contradicting the measurement. With the amine collector present, the force resolves its action directly: it weakens the albite repulsion, the direct-force counterpart of orthoclase's faster, thermodynamically established hydrophobization. Short-range acid–base and hydration forces, rather than the double-layer force, emerge as the dominant contribution distinguishing the two feldspars; the continuum model captures the sign and ordering of this control but not its magnitude.

***Keywords*:** feldspar flotation, albite–orthoclase separation, colloidal-probe AFM, extended DLVO, acid–base (hydration) forces

1. Introduction

Feldspars are among the principal raw materials of the ceramic and glass industries, and the value of a feldspar concentrate is set largely by its alkali balance. For high-strength ceramic bodies, a K_2O/Na_2O ratio above about three is required, which makes the separation of potassium feldspar (microcline/orthoclase) from sodium feldspar (albite) a technological necessity. Because the two minerals are commonly intergrown in the same matrix and are crystallographically and chemically similar, their beneficiation is difficult, and froth flotation has emerged as effectively the only practical route to their selective separation. Cationic-collector flotation of feldspars remains an active area of reagent development (Mohanty et al., 2024; He et al., 2024).

The selectivity of this separation is governed by monovalent cations, sodium in particular. A series of studies has shown that Na^+ addition, typically as NaCl, depresses albite relative to K-feldspar during cationic (amine) flotation (Yanis, 1968; Kovalenko, 1967; Demir et al., 2001; Karagüzel et al., 2005; Gülgönül, 2004). Two complementary mechanisms have been proposed. In the first, Na^+ adsorbs on, or suppresses ion exchange from, the albite surface and thereby hinders amine uptake. In the second, Na^+ acts as a structure-making ion for albite but not for orthoclase, stabilising the interfacial water layer

DOI: 10.37190/ppmp/237557

differently on the two minerals (consistent with the hydrated-cation dependence of hydration forces established for mica; Pashley, 1981). Both pictures imply that the distinction between albite and orthoclase ultimately resides in the balance of interfacial forces, yet for this system those forces have been characterised almost exclusively by indirect means (electrokinetic potentials, contact angles and surface free energies) rather than measured directly.

The interaction between two surfaces in an electrolyte is classically described by DLVO theory, developed independently by Derjaguin and Landau (1941) and Verwey and Overbeek (1948), which sums an attractive Lifshitz–van der Waals (LW) term and a repulsive electrical double-layer (EDL) term. In colloidal systems, this description is often incomplete: hydration, hydrophobic, steric, and other structural forces, absent from the classical formulation, can dominate at short range. Van Oss and co-workers extended the framework by adding a Lewis acid–base (AB) term that captures electron-donor/electron-acceptor interactions in polar media. The resulting extended (x-)DLVO expression has since been applied to a range of mineral, membrane, and biological interfaces (van Oss, 1994; Wu et al., 1999; Brant and Childress, 2002; Sharma and Rao, 2003).

The atomic force microscope (AFM), in the colloidal-probe configuration, provides the means to measure these interactions directly. Since the first colloidal-probe experiments (Ducker et al., 1991; Butt et al., 1995), direct force measurement has become an established tool in mineral processing, and its flotation applications have grown to the point of dedicated reviews (Xing et al., 2018; Wang and Bu, 2026). Colloidal-probe studies have linked measured surface forces to collector-induced hydrophobization and to bubble–particle attachment on oxide and silicate surfaces, interpreting them through DLVO and extended-DLVO theory (Nalaskowski et al., 1999; Drelich et al., 2006; Vigil et al., 1994; Adler et al., 2001). These studies consistently expose a short-range, non-DLVO regime in which structural forces and surface roughness deviate from the classical predictions. More recent measurements continue to resolve electrostatic and hydration contributions on silica and oxide surfaces across a range of ionic strength (Klaassen et al., 2022; Ponce-Gonzalez et al., 2025).

This body of work, however, has been directed almost entirely at sulphide and simple-oxide systems and at collector hydrophobization or bubble attachment. To our knowledge, direct colloidal-probe force measurement has not been applied to the selective separation of the two alkali feldspars. Here, selectivity is set by monovalent-salt modulation of the interfacial forces, beyond the action of the collector alone. It is precisely this gap that the present study addresses.

For the albite–orthoclase system, this experimental link has been missing. In earlier work from our group, the surface free-energy components of the two feldspars, and their change with amine collector and NaCl, were determined by thin-layer wicking (Karagüzel et al., 2005). Their ionic-strength-dependent interaction energies were then computed from electrokinetic data within classical DLVO theory (Güven et al., 2022), and the flotation mechanism was revisited separately (Karagüzel and Çelik, 2022). Both studies explicitly named direct AFM force measurement as the outstanding next step. The thin-layer-wicking study closed with the intent to determine the hydration forces "by utilizing atomic force microscope and the DLVO theory" (Karagüzel et al., 2005). The electrokinetic–DLVO study likewise deferred the acid–base and hydration contributions to a future AFM submission (Güven et al., 2022). The present study delivers that measurement: colloidal-probe AFM force curves between a silica sphere and polished albite and orthoclase surfaces. The curves were acquired as a function of NaCl concentration, at the separation-critical condition, and with the amine collector present. They were decomposed into LW, EDL, and AB contributions through classical and extended DLVO theory. The prior electrokinetic, surface-energy, and microflotation results on the same system (Karagüzel et al., 2005; Güven et al., 2022) provide the independent context against which these forces are interpreted rather than results reproduced here. The aim is twofold. First, to establish by direct measurement, rather than inference, which surface force governs the selectivity between the two feldspars under flotation-relevant conditions. Second, to show how the choice of acid–base combining rule controls the sign of the predicted short-range force, a point of general relevance to extended-DLVO analysis.

2. Material and methods

The only measurements new to the present study are the colloidal-probe AFM force curves (Section 2.5) and their classical/extended-DLVO analysis (Section 2.6). The electrokinetic, microflotation and surface free-energy data (Sections 2.2–2.4) are drawn from earlier studies of the same feldspars (Karagüzel et

al., 2005; Güven et al., 2022) and are summarised here only as the independent context against which the measured forces are interpreted, not as new results.

2.1. Materials

Two provenances of feldspar were used. High-purity albite (Aydın–Çine) and orthoclase (Gördes–Manisa, Turkey), hand-picked as 2–3 cm crystals, were used for the chemical, electrokinetic, contact-angle, and microflotation work; their compositions (ICP, cross-checked by XRF; Table 1) confirm nearly end-member albite (K_2O/Na_2O = 0.016) and orthoclase (K_2O/Na_2O = 5.10). For the AFM force measurements, single-crystal blocks of albite and orthoclase from Utah (USA), supplied as 15–20 cm crystals, were cut into 1 × 1 × 0.5 cm prisms. XRD confirmed albite and orthoclase as the dominant phases, with the parent pegmatite additionally containing muscovite, tourmaline, garnet, sericite, and quartz, and orthoclase exhibiting perthitic albite lamellae. Both provenances are near-end-member feldspars of the same framework-aluminosilicate family (Table 1), so the interfacial chemistry that governs the measured forces is expected to be common to both. The albite-versus-orthoclase force comparison is in any case internally consistent, since both minerals in it are from the single Utah provenance; the Turkish-provenance data enter only as independent context and, through the thin-layer-wicking surface energies, as input to the decomposition (Section 2.6). Samples were sized to −150 + 53 μm for microflotation, −53 μm for electrokinetic tests, and −38 μm (then ground to $d_{50} \approx 7$–10 μm) for thin-layer wicking. The cationic collector, denoted G-TAP, was a fatty alkyl propylene diamine (Genamin-TAP type; Clariant), used at 0.3 mg L^{-1}, the same reagent as in the thin-layer-wicking study of these minerals (Karagüzel et al., 2005). NaCl (Mallinckrodt, analytical reagent grade) served as the indifferent electrolyte for all instrumental measurements, and all solutions were prepared in purified water (18 MΩ cm).

Table 1. Chemical composition of the pure feldspar samples (ICP, confirmed by XRF), wt%

Oxide	Albite	Orthoclase
SiO_2	68.25	66.21
Al_2O_3	19.81	19.15
Na_2O	10.51	2.36
K_2O	0.17	12.04
CaO	0.53	0.08
Fe_2O_3	0.08	0.06
MgO	0.02	0.01
TiO_2	0.10	<0.01
K_2O/Na_2O	0.016	5.10

2.2. Electrokinetic measurements

Zeta potentials were measured by phase-analysis light scattering (Brookhaven Zeta-PALS) at 2 wt% solids. A 0.2 g sample was conditioned in 50 mL of solution for 10 min and allowed to stand 1 min for coarse particles to settle; about ten determinations were averaged per point at 25 ± 2 °C. The ionic-strength dependence (Fig. 1) was measured as a function of NaCl concentration (10^{-4}–1 M) in the bare electrolyte, without collector; the collector was present only in the AFM measurement at the separation condition (Section 2.5) and in the contact-angle work (Section 2.4). (Most pH-profile measurements in the parent study used a Zeta-Meter 3.0 microelectrophoresis unit; the high-ionic-strength NaCl series reported here was acquired with the Zeta-PALS.)

2.3. Microflotation

Microflotation was carried out in a 150 mL column cell (25 × 220 mm) with a 15 μm frit and magnetic stirrer. A 1 g sample was conditioned in 150 mL of collector solution for 10 min and floated for 1 min with nitrogen at 50 cm^3 min^{-1}; floated and unfloated fractions were dried and weighed to give the mass percentage floated.

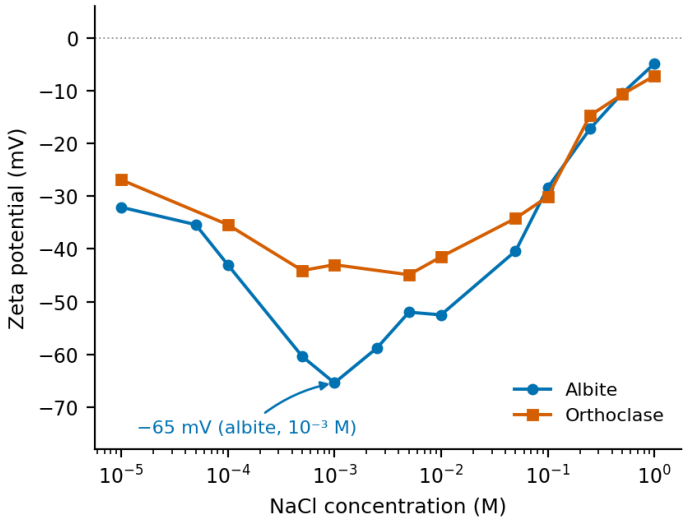

Fig. 1. Electrokinetic zeta potential of albite and orthoclase versus NaCl concentration (bare NaCl, no collector; Zeta-PALS; exact tabulated values from the thesis). Albite passes through a maximum of about −65 mV near 10^{-3} M and the two curves cross near 10^{-1} M

2.4. Surface free energy input (thin-layer wicking)

The dispersive and polar surface free-energy components of albite and orthoclase (γ^{LW} and the Lewis acid–base parameters γ^{+}, γ^{-}) are taken from the thin-layer-wicking (TLW) study of the same minerals by Karagüzel et al. (2005). They are not re-measured in the present work. They serve as input to the force decomposition (Section 2.6) and as context for the collector discussion (Section 3.5). Briefly, in that study the mean pore radius was first obtained from fully-spreading alkanes. Contact angles for water, ethylene glycol and α-bromonaphthalene were then converted to surface-energy components by the van Oss–Chaudhury–Good approach (van Oss, 1994), both for untreated minerals and for surfaces conditioned in G-TAP collector (0.1 and 0.8 mg L^{-1}) and NaCl (10^{-3}–5×10^{-2} M at a constant 0.3 mg L^{-1} amine). With collector addition, the water contact angle increased, and the acid–base component γ^{AB} decreased (Section 3.5). The surface tension of the working media characterises the AFM medium (du Noüy ring method; Krüss K10 tensiometer, 9.45 mm platinum ring, 23 °C). Adding NaCl raised it only slightly (71.4 to 73.1 mN m^{-1} from 0 to 1 M), whereas the collector lowered it (to ~69 mN m^{-1} above 0.8 mg L^{-1}). The medium used in the AFM analysis (0.3 mg L^{-1} collector + 5×10^{-2} M NaCl) measured 69.1 mN m^{-1}.

2.5. AFM force measurements

Direct forces were measured with a Nanoscope III AFM (Digital Instruments) in the colloidal-probe configuration. Mineral surfaces were cut with distilled water only (no organic contaminant), levelled with 400- then 600-mesh SiC abrasive, polished with 1 µm then 0.3 µm alumina (Buehler Micropolish), and sealed into the fluid cell on a steel disc. A 4.8 µm silica sphere was glued to a tipless triangular cantilever (Digital Instruments) with a spring constant of 0.12 N m^{-1}, under a micromanipulator with CCD guidance, and imaged by SEM. The probe geometry, cantilever type, and the spring-constant determination from the cantilever dimensions follow the colloidal-probe procedure of the same laboratory (Nalaskowski et al., 1999; Drelich et al., 2006). Because the spring constant was obtained from the cantilever dimensions rather than by the thermal or Sader method, the absolute force scale carries an estimated ±20–50 % uncertainty; this scales both minerals identically and does not affect the albite–orthoclase comparison. The deflection sensitivity was taken from the constant-compliance region of the deflection–piezo curves, and force–separation profiles were obtained after baseline and hysteresis correction. The zero of separation was defined as the onset of constant compliance, which locates the plane of closest approach rather than a true molecular contact. The polished surfaces have an RMS roughness (~50–100 nm) larger than the range of the short-range forces analysed here. This reference plane therefore carries a corresponding uncertainty on the separation axis. Absolute separations and

contact forces are used only for the relative albite–orthoclase comparison at locally smooth spots, not as absolute quantities. The working solution was equilibrated in the cell ~10 min before measurement. Force curves were acquired over the NaCl range 10^{-4}–1 M at approach/retract velocities of ~1–10 μm s^{-1}, with high-resolution acquisitions at the highest concentrations (5×10^{-2}, 10^{-1}, 1 M); each reported curve is the average of at least six measurements taken at different locations on the surface (Nalaskowski et al., 1999). Natural feldspar surfaces are rough and compositionally heterogeneous, unlike atomically smooth model substrates, so their force curves scatter more from point to point. To guard against this, several curves were averaged at each location, and the measurement was repeated at many independent locations, with extra locations at the separation-critical condition. This follows the practice established for AFM force and adhesion measurement on rough, heterogeneous surfaces (Escobar et al., 2017). In the concentration-series figures (Figs. 2 and 3), the error bars are the standard deviation, showing the full spread of the curves. In the two-mineral comparison figures (Figs. 5 and 6), they are the standard error of the mean ($SEM = SD/\sqrt{N}$, $N \geq 6$). The SEM measures the precision of the location-averaged force and keeps the comparison legible. The underlying standard deviation is retained in Figs. 2 and 3 and quoted in the text (Section 3.3). Reporting the standard deviation for spread and the standard error for the precision of the mean follows established statistical practice (Altman and Bland, 2005) and current AFM data-reporting guidance (Kim et al., 2025). AFM topography gave an RMS roughness of the polished albite and orthoclase surfaces of ~50–100 nm, and the force curves were recorded at locally smooth regions selected from the topography images. All measurements were made at 23 °C and at the natural pH of the solutions (5.6–6.0, close to that of CO_2-equilibrated water).

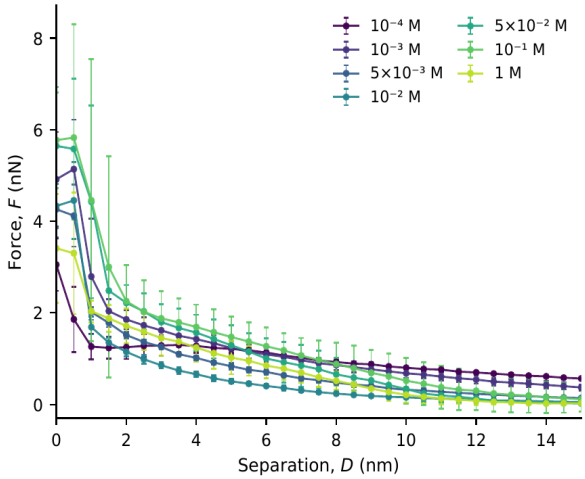

Fig. 2. Albite: surface force versus separation for NaCl 10^{-4}–1 M. Error bars are the standard deviation across N ≥ 6 force curves recorded at different locations on the surface

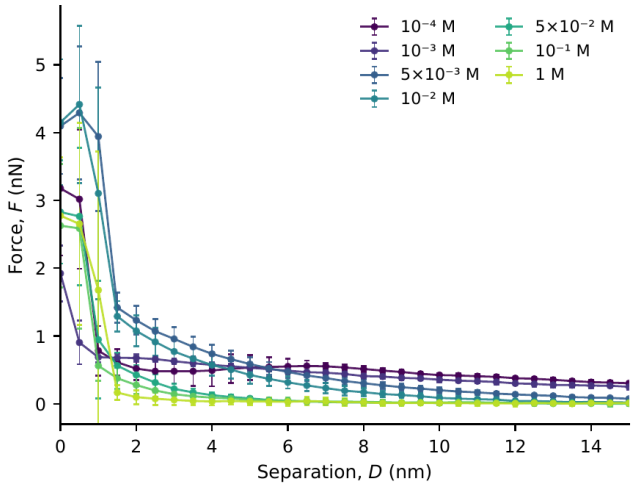

Fig. 3. Orthoclase: surface force versus separation for NaCl 10^{-4}–1 M, with error bars as in Fig. 2 (SD, N ≥ 6)

2.6. Force decomposition (classical and extended DLVO)

Measured force–distance curves were interpreted for a sphere–flat geometry with probe radius R = 2.4 μm (from the 4.8 μm silica sphere), ε_r = 80 and T = 296 K (23 °C). Two analyses were performed. First, each averaged curve was fitted with a constant-potential DLVO expression over the exponential (EDL-dominated) region: a Lifshitz–van der Waals term $F^{\mathrm{LW}}(D) = -\frac{AR}{6D^2}$ plus a screened double-layer term $F^{\mathrm{EDL}}(D) = C\, e^{-\kappa D}$. From this fit the surface potential and Debye length were extracted (Section 3.2). The effective potential reported is the geometric mean $\sqrt{\psi_{\mathrm{silica}} \cdot \psi_{\mathrm{mineral}}}$. Second, the full extended-DLVO decomposition (Sections 3.6–3.7) summed three terms. The Lifshitz–van der Waals term used a Hamaker constant from the LW surface-energy components after van Oss, $A = 12\pi d_0^2\, |\Delta G^{\mathrm{LW}}|$ with d_0 = 0.157 nm. It was evaluated from the intrinsic (untreated) mineral values (silica γ^{LW} = 39.3, water 21.8, albite 39.1 and orthoclase 36 mJ m^{-2}). These give A = 4.7×10^{-21} J (albite) and 4.0×10^{-21} J (orthoclase). The double-layer term F^{EDL} used a constant potential, with κ from the ionic strength. The Lewis acid–base term was $F^{\mathrm{AB}}(D) = 2\pi R\, \Delta G^{\mathrm{AB}}\, e^{(d_0 - D)/\lambda}$, with λ = 0.6 nm. The Hamaker (dispersion) input thus uses the intrinsic mineral energies. This split of conditions is deliberate. The Lifshitz–van der Waals (dispersion) energy is set by the bulk mineral polarisability and is little changed by the sub-monolayer collector. The polar acid–base energy, by contrast, is dominated by the outermost hydrated and collector-modified layer and must be taken at the separation condition. The polar acid–base term instead uses the collector-plus-electrolyte components measured at the separation condition, 5×10^{-2} M NaCl held at 0.3 mg L^{-1} amine (Karagüzel et al., 2005, Table 3). These are: albite γ^{LW} = 22.3, γ^{+} = 0.18, γ^{-} = 21.3 mJ m^{-2}; orthoclase γ^{LW} = 21.5, γ^{+} = 0.97, γ^{-} = 13.0 mJ m^{-2}; and the silica probe γ^{LW} = 40.9, γ^{+} = 0.1, γ^{-} = 62.4 mJ m^{-2} (van Oss, 1994). ΔG^{AB} was evaluated both with the rigorous van Oss combining rule (using γ^{+}, γ^{-}) and with the simplified rule adopted in the original analysis. Computations were performed as a function of separation and overlaid on the AFM data.

3. Results and discussion

3.1. Ionic-strength dependence of the surface forces

Figs. 2 and 3 show the force between the silica probe and the albite and orthoclase surfaces as a function of NaCl concentration. For both minerals, the interaction is repulsive over the whole measured range, and its behaviour with added electrolyte is best understood by separating the *range* of the force from its *short-range magnitude*. The range is characterised by an exponential decay length fitted between 2 and 15 nm. It contracts monotonically as the ionic strength rises. For albite it falls from 14.3 nm at 10^{-4} M to 4.3 nm at 10^{-2} M and 2.8 nm at 5×10^{-2} M. For orthoclase, it falls from 24.1 to 3.2 nm over the same interval. These values are of the same order as the theoretical Debye length (30.4, 3.0, and 1.4 nm, respectively), tracking it most closely at intermediate concentration, which confirms that the long-range part of the interaction is an electrical double-layer force progressively compressed as the electrolyte screens the surface charge.

The short-range magnitude, by contrast, does not decrease monotonically. For albite, the force at 5 nm falls from 1.2 nN at 10^{-4} M to 0.5 nN at 10^{-2} M but then rises again to 1.3–1.5 nN at 5×10^{-2}–10^{-1} M. A purely DLVO interaction cannot reproduce this rebound, because double-layer compression can only weaken the repulsion. The strong short-range force re-emerges precisely where the Debye length has collapsed below ~1.5 nm. This is the first sign that a non-DLVO, structural contribution operates at these separations, consistent with the hydration forces reported for hydrophilic silica and oxide surfaces at high ionic strength (Israelachvili and Pashley, 1983; Valle-Delgado et al., 2005; Klaassen et al., 2022; Ponce-Gonzalez et al., 2025).

3.2. Surface potentials and Debye lengths from the force curves

To quantify the double-layer contribution identified in Section 3.1, a constant-potential DLVO expression (EDL + van der Waals) was fitted to each averaged force curve, so that the surface potential and Debye length were obtained directly from the data rather than assumed (Fig. 4). The fitted Debye length reproduces the theoretical value across the intermediate range (10^{-3}–5×10^{-2} M; Fig. 4b), confirming that the long-range force is a genuine electrical double-layer interaction and providing an

internal consistency check on the measurements. The fit degrades only at 10^{-4} M, where the interaction extends beyond the measured window, and above 10^{-1} M, where the double layer is compressed to below 1 nm, and the residual structural force contaminates the exponential region. The extracted effective potential is the geometric mean $\sqrt{\psi_{\text{silica}} \cdot \psi_{\text{mineral}}}$ of the constant-potential fit. It decreases monotonically with ionic strength for both minerals, from ~33 to ~15 mV for albite and ~24 to ~8 mV for orthoclase between 10^{-4} and 10^{-1} M. This is expected for progressive double-layer screening and charge regulation (Fig. 4a).

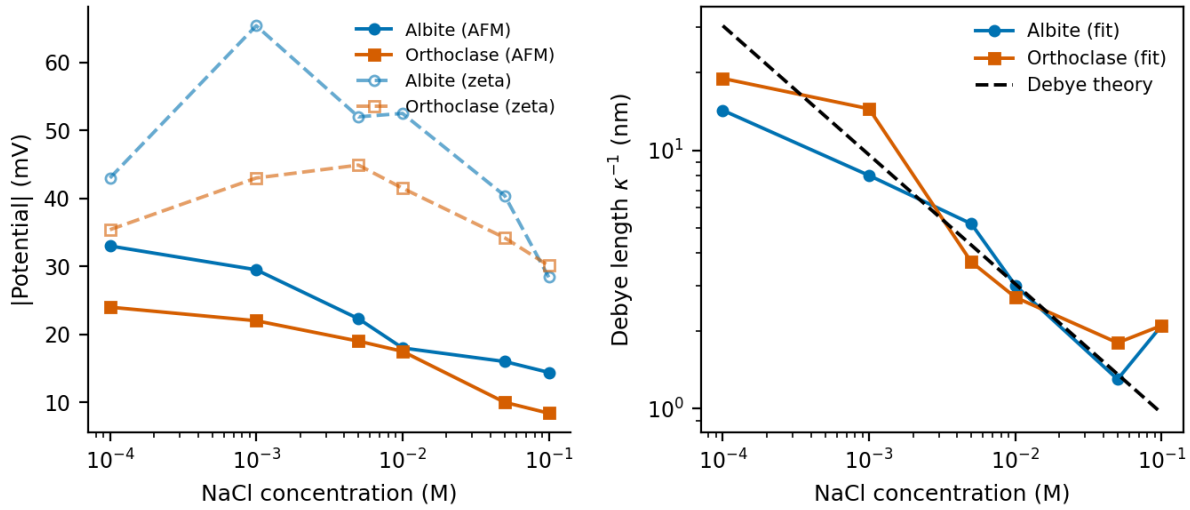

Fig. 4. (a) AFM-extracted effective surface potential versus electrokinetic zeta potential and (b) fitted versus theoretical Debye length, as a function of NaCl concentration

Comparison with the electrokinetic measurements ties the two independent probes together (Fig. 4a; cf. the zeta-potential data, Fig. 1), both acquired in the bare NaCl electrolyte. The mineral ordering is preserved (albite carries the more negative potential than orthoclase over essentially the whole range), and this difference persists at the high-ionic-strength, separation-relevant end (16 vs 10 mV at 5×10^{-2} M and 15 vs 8 mV at 10^{-1} M). The electrokinetic zeta potentials, now read from the exact tabulated data, agree where they remain resolved: albite is the more negative mineral at 5×10^{-2} M (−40.4 vs −34.2 mV). The two curves converge and cross only at and above 10^{-1} M (−28.4 vs −30.1 mV). There the electrophoretic measurement, sensitive only to the outer slip plane, can no longer distinguish the two minerals. The direct-force measurement, by contrast, keeps the albite–orthoclase potential difference resolved in this compressed-double-layer regime. As expected, the AFM-extracted potentials are systematically smaller than the zeta potentials, which reach ~65 mV for albite and pass through a maximum near 10^{-3} M. The force-curve value is a diffuse-layer potential referred to the plane of closest fit. It is reduced further by its geometric-mean combination with the silica probe and by charge regulation between the dissimilar surfaces (Behrens and Grier, 2001). The agreement in sign, mineral ordering, and ionic-strength trend, together with the quantitative match of the Debye length, shows that the same double-layer physics governs both the electrokinetic and the direct-force behaviour. The force measurement additionally holds the albite–orthoclase potential difference resolved at the high ionic strengths where the zeta potentials converge.

3.3. Force difference at the separation-critical condition

Fig. 5 compares the two minerals at the condition where selective flotation is observed (5×10^{-2} M NaCl with 0.3 mg L^{-1} collector). This ionic strength, rather than 10^{-2} M, was adopted because the difference between the two was not sharp, and 5×10^{-2} M coincided with the NaCl concentration at which selective separation was reported in the parent flotation studies (Demir et al., 2001; Gülgönül, 2004). A systematic difference appears at short range: at every separation below ~7 nm the albite force exceeds that of orthoclase, by 1.7 nN at contact and ~1.3 nN at 1 nm, with the gap closing to within scatter beyond ~10 nm. The run-to-run scatter at any single separation is large, with a standard deviation comparable to

the mean (for example, albite 4.2 ± 2.2 nN and orthoclase 2.4 ± 1.4 nN at contact; mean ± SD, N ≥ 6), which reflects the local heterogeneity of the polished surfaces. At any single separation, the mineral difference is therefore about one standard deviation and is not resolved on its own: a Welch t-test at contact, appropriate for the unequal variances, gives $p \approx 0.09$ (West, 2021). The evidence for selectivity is the consistency of the offset across separations rather than the value at any single point. Albite exceeds orthoclase at every measured separation below ~7 nm, and this ordering is reproduced in the location-averaged curves, each built from N ≥ 6 force curves recorded at independent surface locations, which are the true experimental replicates (Specht et al., 2025). Successive separations along one force curve are strongly autocorrelated, so we do not treat them as independent trials. The selectivity signal resides in the systematic, sign-consistent offset of the location-averaged curves, resolved within the standard error ($SEM = SD/\sqrt{N}$; Figs 5 and 6). A location-resolved test on a single summary statistic per location, for example the near-contact force, would place this comparison on a fully independent footing and is a natural refinement of the present analysis. Albite therefore experiences the systematically stronger repulsion under flotation conditions. This is the direct, force-level counterpart of the electrokinetic and thermodynamic selectivity established for this system: the more negative potential of Section 3.2 and the ~8 mJ m^{-2} larger surface free energy of albite. At the level of individual surface forces, it is consistent with albite being the more dispersed, less collector-receptive, and hence depressed mineral.

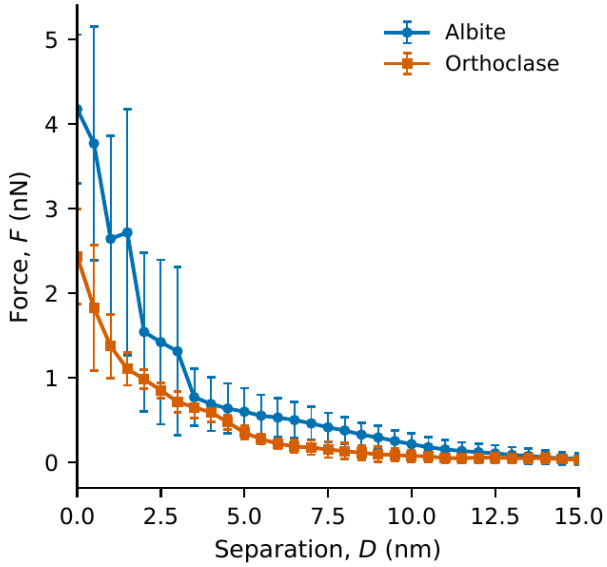

Fig. 5. Albite versus orthoclase at the separation-critical condition (5×10^{-2} M NaCl + 0.3 mg L^{-1} collector). Error bars are the standard error of the mean ($SEM = SD/\sqrt{N}$, N ≥ 6)

3.4. Collector effect on the surface force

The curves in Sections 3.1–3.3 characterise the electrolyte-modulated interaction; the flotation environment additionally contains the amine collector. To isolate its effect, the force at the separation condition (5×10^{-2} M NaCl) was measured for each mineral both in the bare electrolyte and after adding 0.3 mg L^{-1} G-TAP (Fig. 6). The collector acts in opposite senses on the two feldspars. On albite, it weakens the repulsion across the whole range (the near-contact force falls from 5.6 to 4.2 nN and the 5 nm force from 1.3 to 0.6 nN), as expected when adsorbing amine partially neutralises the surface charge and erodes the hydration repulsion. On orthoclase, the near-contact force is essentially unchanged, but a broadened, structured repulsion emerges over 1–5 nm (rising from ~0.1 to ~0.4 nN at 3–5 nm), the signature of an adsorbed amine layer of finite range rather than of simple charge screening. As in Section 3.3, the run-to-run scatter at any single separation is large (SD comparable to the mean, N ≥ 6), so these values describe systematic trends in the location-averaged curves rather than differences resolved at any individual point. Because the probe is a silica sphere and not an air bubble, these curves report the collector's effect on the mineral–silica interaction rather than on bubble attachment directly. The independently measured wettability and flotation data for this system (Sections 3.5, 3.8) provide the probe-independent link to floatability.

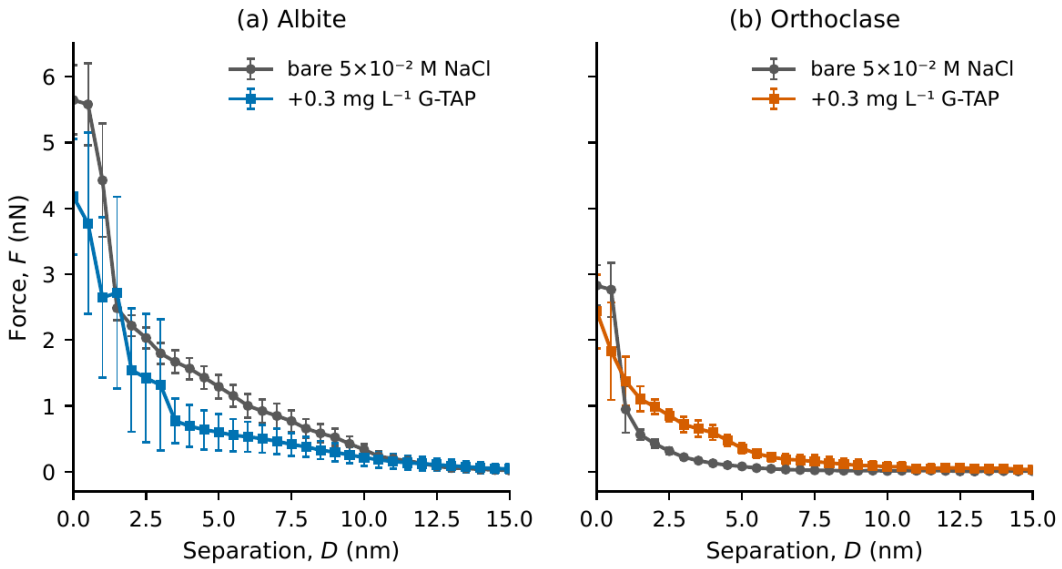

Fig. 6. Collector effect on the surface force at 5×10⁻² M NaCl: bare electrolyte versus +0.3 mg L⁻¹ G-TAP, for albite and orthoclase. Error bars SEM (N ≥ 6)

3.5. Consistency with collector-induced hydrophobization

The opposite responses of the two minerals to the collector (Section 3.4) are the direct-force counterpart of the wettability and surface free energy previously measured on the same feldspars by thin-layer wicking (Karagüzel et al., 2005). In that work, the water contact angle increased with G-TAP dose on both minerals, but faster on orthoclase in the low-dose, selectivity-relevant regime (66° vs 57° for albite at 0.1 mg L^{-1}); the two converged only at high dose (74–75° at 0.8 mg L^{-1}). Meanwhile, the acid–base component γ^{AB}, which supplies the short-range hydration repulsion, collapsed from ~17 to ~0.2 mJ m^{-2} as the amine adsorbed. The collector that hydrophobizes orthoclase earliest, and that collapses its γ^{AB}, is thus the same collector that erodes the short-range repulsion in the force curves. Because contact angle and force are independent probes, their agreement removes the ambiguity of interpreting the silica-probe force alone, and the collector-plus-electrolyte γ components measured at the separation condition (Karagüzel et al., 2005) serve directly as the input to the extended-DLVO decomposition (Section 3.6).

3.6. Extended-DLVO decomposition and the acid–base term

To identify which force governs this difference, the measured curves were decomposed into LW, EDL and AB contributions for a sphere–flat geometry (Fig. 7). The polar surface free-energy components used as input were the thin-layer-wicking values for albite and orthoclase at the separation condition, 5×10⁻² M NaCl held at 0.3 mg L^{-1} amine, matching the collector-plus-electrolyte condition of the AFM measurement (Karagüzel et al., 2005, Table 3). These components were measured on the Turkish-provenance crystals and are used as representative end-member values, since the decomposition turns on the albite–orthoclase contrast in polar surface energy rather than on absolute provenance. The quantitative albite–orthoclase ΔG^{AB} ratio therefore inherits the provenance of these surface-energy inputs rather than that of the force measurement. We read it as an end-member contrast, and direct thin-layer-wicking or contact-angle measurement on the Utah surfaces would remove this residual assumption. Across the decomposition the LW term is small and attractive (Hamaker constant A = 4.7×10⁻²¹ J for albite and 4.0×10⁻²¹ J for orthoclase), the EDL term provides the intermediate-range repulsion, and the AB term dominates below ~3 nm.

The sign of the AB term depends critically on the combining rule. With the rigorous van Oss expression, using the electron-donor and electron-acceptor parameters, the AB interaction is strongly repulsive for both minerals (ΔG^{AB} = +22 mJ m^{-2} for albite, +9.5 for orthoclase, computed from the Karagüzel et al. (2005) components against the silica probe). This is the expected hydration-type repulsion between two hydrophilic surfaces in water. The van Oss acid–base term and a structural hydration force are not strictly identical: the first is a continuum electron-donor/acceptor free energy,

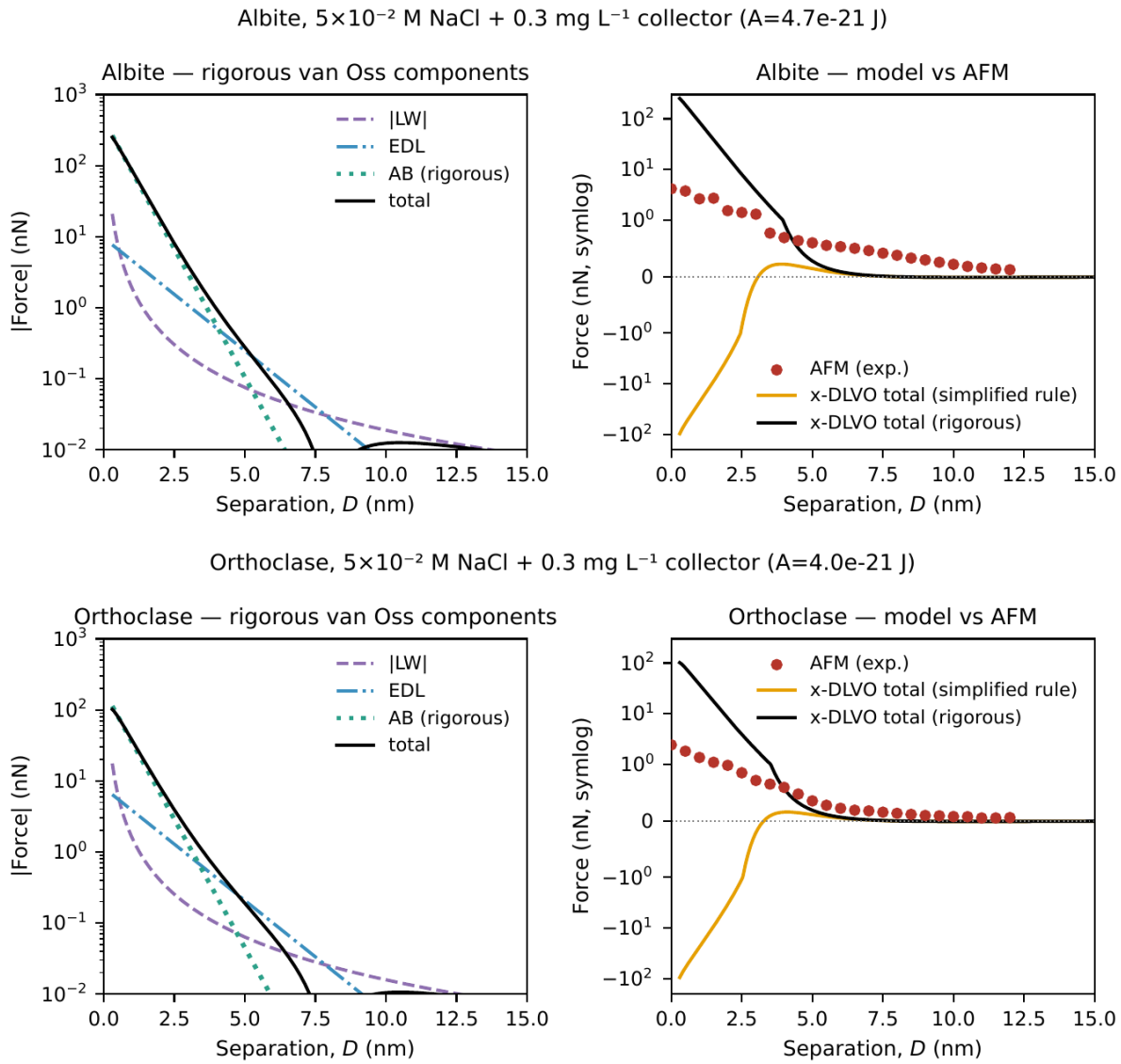

Fig. 7. Extended-DLVO decomposition (LW, EDL and AB terms; rigorous versus simplified-rule totals against the AFM data) for (a) albite and (b) orthoclase

the second arises from the molecular layering of interfacial water. Here they share the same short range and the same repulsive sign, and we use 'acid–base (hydration-type)' for this combined short-range polar repulsion rather than to equate the two mechanisms. This is the physically consistent result: it has the same (repulsive) sign as every measured force curve, and the more than twofold-larger albite value mirrors the flotation selectivity. The simplified combining rule adopted in the original analysis treats the composite γ^{AB} as a single dispersion-like quantity, rather than as separate electron-donor and electron-acceptor parameters. It instead returns an attractive AB term (of order −10 mJ m^{-2}, the precise magnitude being combining-rule dependent), even when the correct polar surface tension of water is used. As Fig. 7 shows, this attractive form drives the predicted total force negative at contact, in direct contradiction to the repulsion measured by AFM. We therefore regard the repulsive, rigorously-combined AB term as the correct description and the earlier attractive result as an artefact of the simplified combining rule. This is not specific to feldspar. The same simplification treats the composite γ^{AB} as a single dispersion-like quantity, rather than resolving it into separate electron-donor (γ^-) and electron-acceptor (γ^+) parameters. It recurs in applied extended-DLVO analyses across mineral, membrane and biological interfaces, so the sign reversal demonstrated here is a general caution (Della Volpe and Siboni, 2000). Wherever the acid–base term governs the short-range interaction, the

combining rule must retain the separate γ^+ and γ^- parameters, or the predicted force can acquire the wrong sign.

Neither formulation reproduces the *magnitude* of the measured force: the rigorous AB term overpredicts the contact force by more than an order of magnitude. This is a known limitation of the continuum van Oss treatment. It uses bulk-water polar parameters and a single exponential decay, and it ignores surface roughness, discrete hydration structure, and partial collector coverage. The polished surfaces had an RMS roughness of ~50–100 nm, exceeding both the Debye length and the range of the short-range interaction, although the curves were recorded at locally smooth spots. The decomposition should thus be read as identifying the *dominant selectivity-determining force* (the short-range acid–base/hydration repulsion, stronger on albite) rather than as a quantitative fit.

3.7. Hydration forces and the DLVO residual

Because the van Oss AB term already embodies the hydration interaction, an independent estimate was made by subtracting the classical DLVO force (LW+EDL) from the measured curves (Fig. 8). Consistent with the fits of Section 3.2, the double-layer-subtracted residual leaves a positive, short-range (<1.5 nm) excess that grows with electrolyte and decays over ~0.5–1 nm, the range expected for a hydration force between hydrophilic silicate surfaces (Israelachvili and Pashley, 1983; Valle-Delgado et al., 2005). With constant-potential parameters reconstructed for the amine condition (surface potentials taken from the bare-electrolyte constant-potential fits of Section 3.2 at 5×10^{-2} M and the Debye length fixed by the ionic strength), the residual becomes small and sign-ambiguous below ~2 nm. Classical DLVO computed with those potentials therefore already meets or exceeds the measured repulsion. This is consistent with a partial short-range attraction from amine-induced hydrophobization, most pronounced on the better-floating orthoclase. Over 3–7 nm a small positive residual (~0.3–0.4 nN) is resolved for albite but not for orthoclase, the closest data-level signature of an excess, hydration-like repulsion specific to the more hydrophilic mineral. This residual is the small difference between two larger quantities and is sensitive to the assumed surface potentials. The data therefore support hydration forces as *qualitatively present and mineral-distinguishing*, but do not permit their quantitative isolation. This is a more defensible position than fitting a separate empirical hydration term, which would double-count the acid–base contribution.

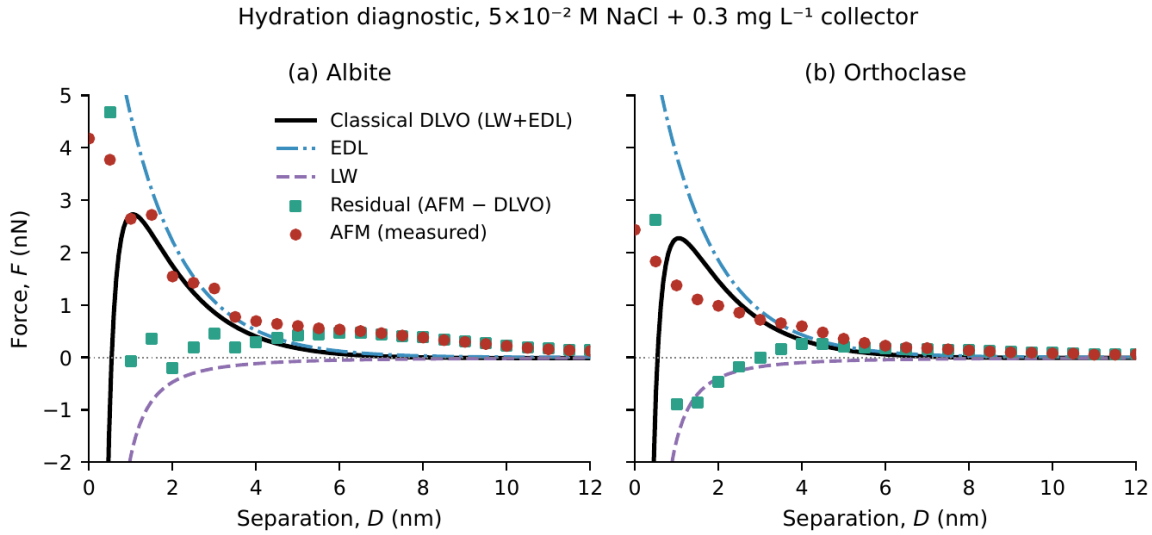

Fig. 8. Hydration diagnostic: measured force versus classical DLVO (LW+EDL) and the residual

3.8. Mechanistic picture

The surface-force account is consistent with the microflotation behaviour previously reported for the same system (Karagüzel et al., 2005). Without added electrolyte, both feldspars float once the amine dose is high enough, with essentially no selectivity. Selectivity emerges only on adding NaCl, which

depresses albite more strongly than orthoclase. The direct-force measurements reported here supply the surface-force mechanism that underlies that established flotation behaviour.

Taken together, the measurements resolve the selectivity of Na/K-feldspar flotation into a sequence of surface forces. Added Na^+ compresses the double layer of both minerals, but more strongly suppresses collector uptake on albite, whose lattice Na^+ precludes ion exchange. At the separation-critical ionic strength the residual selectivity is carried by a short-range acid–base/hydration repulsion that is markedly stronger on albite. By then the screened double-layer force is too short-ranged to contribute. Albite consequently retains a more hydrated, repulsive, collector-resistant interface and is depressed, whereas orthoclase, less hydrated and partially hydrophobised by the amine, floats. This direct-force account is consistent with, and completes, the electrokinetic and surface-thermodynamic picture previously reported for this system.

4. Conclusions

Colloidal-probe AFM force measurements, interpreted through classical and extended DLVO theory, resolve the selective flotation of albite from orthoclase into a defined sequence of surface forces. They provide the direct experimental link that previous electrokinetic and thermodynamic studies of this system had identified as missing.

The principal findings are as follows. (i) For both minerals, the silica–mineral interaction is repulsive, and added NaCl compresses its range in agreement with the Debye length in trend and to within a factor of about two, confirming that the long-range interaction is an electrical double-layer force. (ii) Fitting each force curve with constant-potential DLVO returns effective surface potentials that reproduce the electrokinetic ordering (albite more negative than orthoclase) and, at high ionic strength, resolve a mineral-distinguishing potential difference not apparent in the electrophoretic zeta potentials. (iii) The short-range repulsion does not vanish as the double layer is screened; it re-emerges at high ionic strength, revealing a non-DLVO structural contribution. (iv) At the separation-critical condition (5×10^{-2} M NaCl, 0.3 mg L^{-1} collector), albite exhibits a systematically stronger short-range repulsion than orthoclase, consistent in sign across the near-contact regime and resolved in the location-averaged curves, the direct force-level expression of the flotation selectivity. (v) A rigorous van Oss decomposition assigns this difference to a repulsive Lewis acid–base (hydration-type) force more than twice as large on albite as on orthoclase; the attractive acid–base term obtained with a simplified combining rule in earlier work is inconsistent with the measured repulsion and is not supported. (vi) Direct subtraction of the classical DLVO force does not isolate a distinct hydration term, which the data support as qualitatively present and mineral-distinguishing but not quantitatively separable given the uncertainty in surface potentials. (vii) The collector-conditioned force completes the mechanism: adding the amine weakens the albite repulsion, the direct-force counterpart of the faster hydrophobization and acid–base (γ^{AB}) collapse of orthoclase established by thin-layer wicking for this system (Karagüzel et al., 2005), while NaCl selectively depresses albite in microflotation.

Mechanistically, once the double layer is screened by the electrolyte, the residual selectivity between the two feldspars is carried by a short-range acid–base/hydration repulsion that is stronger on the more hydrophilic albite, keeping its interface dispersed and collector-resistant while orthoclase, partially hydrophobised by the amine, floats. The continuum extended-DLVO model captures the sign and ordering of this controlling force but overestimates its magnitude. A quantitative account of feldspar selectivity will therefore require treatments that incorporate surface roughness, discrete interfacial-water structure and local collector coverage. Natural next steps are AFM mapping of the polished surfaces and mineral–mineral (rather than silica-probe) force measurements.

Acknowledgments

The authors thank Prof. Dr. Ender Sönmez for supervising the doctoral thesis on which this work is based, and Prof. Dr. Mehmet Sabri Çelik for his guidance and mentorship throughout their academic careers. They also thank Prof. J. D. Miller and Dr. J. Nalaskowski (University of Utah) for hosting and supporting the colloidal-probe AFM measurements. This research did not receive any specific grant from funding agencies in the public, commercial, or not-for-profit sectors.

References

ADLER, J.J., RABINOVICH, Y.I., MOUDGIL, B.M., 2001. *Origins of the non-DLVO force between glass surfaces in aqueous solution.* J. Colloid Interface Sci. 237, 249-258. DOI 10.1006/jcis.2001.7466.

ALTMAN, D.G., BLAND, J.M., 2005. *Standard deviations and standard errors.* BMJ 331(7521), 903. DOI 10.1136/bmj.331.7521.903.

BEHRENS, S.H., GRIER, D.G., 2001. *The charge of glass and silica surfaces.* J. Chem. Phys. 115(14), 6716-6721. DOI 10.1063/1.1404988.

BRANT, J.A., CHILDRESS, A.E., 2002. *Membrane–colloid interactions: comparison of extended DLVO predictions with AFM force measurements.* Environ. Eng. Sci. 19, 413-427. DOI 10.1089/109287502320963409.

BUTT, H.J., JASCHKE, M., DUCKER, W.A., 1995. *Measuring surface forces in aqueous electrolyte solution with the atomic force microscope.* Bioelectrochem. Bioenerg. 38, 191-201. DOI 10.1016/0302-4598(95)01800-T.

DELLA VOLPE, C., SIBONI, S., 2000. *Acid–base surface free energies of solids and the definition of scales in the Good–van Oss–Chaudhury theory.* J. Adhes. Sci. Technol. 14(2), 235-272. DOI 10.1163/156856100742546.

DEMIR, C., ABRAMOV, A.A., ÇELIK, M.S., 2001. *Flotation separation of Na-feldspar from K-feldspar by monovalent salts.* Miner. Eng. 14, 733-740. DOI 10.1016/S0892-6875(01)00069-3.

DERJAGUIN, B.V., LANDAU, L.D., 1941. *Theory of the stability of strongly charged lyophobic sols and of the adhesion of strongly charged particles in solutions of electrolytes.* Acta Physicochim. URSS 14, 633-662.

DRELICH, J., LONG, J., XU, Z., MASLIYAH, J., NALASKOWSKI, J., BEAUCHAMP, R., LIU, Y., 2006. *AFM colloidal forces measured between microscopic probes and flat substrates in nanoparticle suspensions.* J. Colloid Interface Sci. 301, 511-522. DOI 10.1016/j.jcis.2006.05.044.

DUCKER, W.A., SENDEN, T.J., PASHLEY, R.M., 1991. *Direct measurement of colloidal forces using an atomic force microscope.* Nature 353, 239-241. DOI 10.1038/353239a0.

ESCOBAR, J.V., GARZA, C., CASTILLO, R., 2017. *Measuring adhesion on rough surfaces using atomic force microscopy with a liquid probe.* Beilstein J. Nanotechnol. 8, 813-825. DOI 10.3762/bjnano.8.84.

GÜLGÖNÜL, İ., 2004. *Mechanism of monovalent and bivalent ions on the separation of sodium feldspar from potassium feldspar by cationic flotation.* PhD thesis, Istanbul Technical University, Istanbul.

GÜVEN, O., CAN, M.F., KARAGÜZEL, C., 2022. *The effect of NaCl concentration on the interaction energy between feldspar minerals.* Physicochem. Probl. Miner. Process. 58(5), 151031. DOI 10.37190/ppmp/151031.

HE, Y., REN, Z., ZHU, H., ZHENG, R., LI, M., SONG, Y., CHEN, Z., 2024. *Application of dodecyl amine/sodium petroleum sulfonate mixed collector in quartz–feldspar flotation separation.* Physicochem. Probl. Miner. Process. 60(1), 185553. DOI 10.37190/ppmp/185553.

ISRAELACHVILI, J.N., PASHLEY, R.M., 1983. *Molecular layering of water at surfaces and origin of repulsive hydration forces.* Nature 306, 249-250. DOI 10.1038/306249a0.

KARAGÜZEL, C., CAN, M.F., SÖNMEZ, E., ÇELIK, M.S., 2005. *Effect of electrolyte on surface free energy components of feldspar minerals using thin-layer wicking method.* J. Colloid Interface Sci. 285(1), 192-200. DOI 10.1016/j.jcis.2004.11.018.

KARAGÜZEL, C., ÇELIK, M.S., 2022. *Revisiting flotation mechanisms of the selective separation of alkali feldspars in the presence of NaCl.* Physicochem. Probl. Miner. Process. 58(5), 149928. DOI 10.37190/ppmp/149928.

KIM, E., RAMOS FIGUEROA, A.L., SCHROCK, M., ZHANG, E., NEWCOMB, C.J., BAO, Z., MICHALEK, L., 2025. *A guide for nanomechanical characterization of soft matter via AFM: from mode selection to data reporting.* STAR Protoc. 6, 103809. DOI 10.1016/j.xpro.2025.103809.

KLAASSEN, A., LIU, F., MUGELE, F., SIRETANU, I., 2022. *Correlation between electrostatic and hydration forces on silica and gibbsite surfaces: an atomic force microscopy study.* Langmuir 38(3), 914-926. DOI 10.1021/acs.langmuir.1c02077.

KOVALENKO, V.I., 1967. *Flotation beneficiation of feldspathic raw material by using potassium and sodium chloride.* Obogashch. Rud 12(1), 8-11.

MOHANTY, K., OLIVA, J., ALFONSO, P., SAMPAIO, C.H., ANTICOI, H., 2024. *A comparative study of quartz and potassium feldspar flotation process using different chemical reagents.* Minerals 14(2), 167. DOI 10.3390/min14020167.

NALASKOWSKI, J., VEERAMASUNENI, S., HUPKA, J., MILLER, J.D., 1999. *AFM measurements of hydrophobic forces between a polyethylene sphere and silanated silica plates: the significance of surface roughness.* J. Adhesion Sci. Technol. 13(12), 1519-1533. DOI 10.1163/156856199X00622.

PASHLEY, R.M., 1981. *Hydration forces between mica surfaces in aqueous electrolyte solutions.* J. Colloid Interface Sci. 80(1), 153-162. DOI 10.1016/0021-9797(81)90171-5.

PONCE-GONZALEZ, L.N., SUDJARWO, W.A.A., TOCA-HERRERA, J.L., 2025. *Measuring colloidal forces with atomic force microscopy 1: salt influence on hydrophobic and hydrophilic interactions.* Microsc. Res. Tech. 88(6), 1626-1634. DOI 10.1002/jemt.24832.

SHARMA, P.K., RAO, K.H., 2003. *Adhesion of Paenibacillus polymyxa on chalcopyrite and pyrite: surface thermodynamics and extended DLVO theory.* Colloids Surf. B 29, 21-38. DOI 10.1016/S0927-7765(02)00180-7.

SPECHT, A., KRÄMER, D., HELFRICHT, N., PAPASTAVROU, G., 2025. *How much data are enough? Toward statistically robust adhesion experiments by atomic force microscopy.* Langmuir 41(10), 6515-6527. DOI 10.1021/acs.langmuir.4c03519.

VALLE-DELGADO, J.J., MOLINA-BOLÍVAR, J.A., GALISTEO-GONZÁLEZ, F., GÁLVEZ-RUIZ, M.J., FEILER, A., RUTLAND, M.W., 2005. *Hydration forces between silica surfaces: experimental data and predictions from different theories.* J. Chem. Phys. 123, 034708. DOI 10.1063/1.1954747.

VAN OSS, C.J., 1994. *Interfacial Forces in Aqueous Media.* Marcel Dekker, New York.

VERWEY, E.J.W., OVERBEEK, J.Th.G., 1948. *Theory of the Stability of Lyophobic Colloids.* Elsevier, Amsterdam.

VIGIL, G., XU, Z., STEINBERG, S., ISRAELACHVILI, J., 1994. *Interactions of silica surfaces.* J. Colloid Interface Sci. 165, 367-385. DOI 10.1006/jcis.1994.1242.

WANG, G., BU, X., 2026. *Particle–bubble interactions in the flotation process.* Minerals 16(4), 383. DOI 10.3390/min16040383.

WEST, R.M., 2021. *Best practice in statistics: use the Welch t-test when testing the difference between two groups.* Ann. Clin. Biochem. 58(4), 267-269. DOI 10.1177/0004563221992088.

WU, W., GIESE, R.F., VAN OSS, C.J., 1999. *Stability versus flocculation of particle suspensions in water: correlation with the extended DLVO approach for aqueous systems, compared with classical DLVO theory.* Colloids Surf. B 14, 47-55. DOI 10.1016/S0927-7765(99)00023-5.

XING, Y., GUI, X., CAO, Y., BABEL, B., RUDOLPH, M., WEBER, S., KAPPL, M., BUTT, H.-J., 2018. *The application of atomic force microscopy in mineral flotation: a critical review.* Adv. Colloid Interface Sci. 256, 373-392. DOI 10.1016/j.cis.2018.01.004.

YANIS, N.A., 1968. *Froth flotation procedure for separating potassium feldspar from sodium feldspar.* USSR Patent 227234.